Post-Test Corrosion Analysis of High-Temperature Thermal Energy Storage Capsules

H. Fathollahnejad, B.-H. Tsao, R. Ponnappan, and D. Jacobson

Thermal energy storage capsules have been freeze-thaw cycled in vacuum at 1000 ± 100 K. The capsules were fabricated from Inconel 617® (Inco Alloys International, Inc.) and contained eutectic fluoride mixtures of sodium, magnesium, lithium, and potassium. Samples that were thermal cycled for 20,000 and 30,000 hr were analyzed for corrosion effects. Radiography indicated neither flaws nor inhomogeneities, and there were no significant microstructural changes in the container alloy. The microstructural damage penetrating the inside surface was as deep as 120 m and that penetrating the outside surface was approximately 150 m. Microprobe results on the containers revealed a concentration gradient of alloying elements. The aluminum concentration was reduced from 1.34% in the original matrix to 0.4% at 10 m from the inside surface, and chromium was reduced from a nominal value of 23% to 10% at the outer surface. The depletion of aluminum and chromium from the outer surface was due to vacuum vaporization at elevated temperature. X-ray diffraction revealed the formation of possible protective films consisting of $MgNaF_3$ and MgF_2. The measured and theoretically predicted concentrations of aluminum and chromium were in good agreement. It was concluded that the corrosion process is a solid-state diffusion-dominated process and an expected lifetime of 5 to 7 years is a reasonable estimate.

Keywords:
corrosion, storage capsules, thermal energy

1. Introduction

FOR the past 20 years, thermal energy storage (TES) in the form of latent heat of fusion has attracted scientific and engineering efforts on solar dynamic applications to provide electric power for space stations and for future space missions. The technique has the potential to replace conventional electrochemical energy storage methods. Thermal energy storage could meet the power demand of a spacecraft effectively during an eclipse. This form of energy storage is advantageous relative to other forms because it is possible to obtain (1) maximum enthalpy per unit volume, (2) minimum temperature variation, and (3) high efficiency (exceeding 90%) compared to NiCd batteries with 70 to 75%.[1]

A solid-to-liquid phase change is an ideal form of thermal energy storage for this purpose, because energy density (kJ/g) is generally much higher than solid-to-solid phase changes, and a high-strength containment vessel to accommodate the pressure buildup from a liquid-to-vapor transformation is not required.[2] Multicomponent fluoride salt mixtures are strong candidates for thermal energy storage purposes. These salt mixtures have melting points near 1000 K. The heats of fusion of these salt mixtures are well above the minimum requirement of 0.4 kJ/g.[2]

Inconel 617 (nominal composition: 55 wt.% Ni, 22 wt.% Cr, 13 wt.% Co, 8 wt.% Mo, 1.34 wt.% Al, and the remainder Fe, C, and Ti) was selected as a reference containment material because it complies with the thermodynamic considerations discussed in Misra.[2] Because there were no reliable experimental data on the corrosion behavior of Inconel 617 exposed to fluoride salts at high temperatures, thermal energy storage experiments were conducted at the Air Force Wright Laboratory.[3] Ultrapure salt eutectics—A (LiF, MgF_2, and KF), B (LiF, MgF_2, and NaF), and C (LiF and MgF_2)—were put into thermal energy storage capsules made of Inconel 617 and were then thermally cycled. Every 10,000 hr, three of the capsules containing the three different eutectic salts were removed for corrosion analysis. Nine of these capsules (tested for 10,000, 20,000, and 30,000 hr), were transferred to Arizona State University for post-test corrosion analysis. Samples tested for 10,000 hr were analyzed and found to have very little damage resulting from fluoride salt reaction with the containers.[4] The present work describes the corrosion analysis of the capsules after 20,000 and 30,000 hr of testing. Qualitative and semiquantitative analyses were performed on the samples to identify the probable corrosion mechanism and to predict lifetime.

H. Fathollahnejad and **D. Jacobson,** Chemical, Bio and Material Engineering Dept., Arizona State University, Tempe, Arizona; and **B.H. Tsao** and **R. Ponnappan**, UES, Inc., Dayton, Ohio.

2. Experimental Procedures

2.1 *Capsule Preparation*

Segments of 7.62-cm long and 2.54-cm diameter Inconel 617 tubing with 0.16-cm wall thickness were cut to form the containment capsule. The ends were machined to fit end caps machined out of bar stock of the same material. After thorough cleaning, the bottom end caps were electron-beam welded in place and cleaned again before placing inside an argon-filled glove box (oxygen content <1 ppm). The ultrapure fluoride salts (Tables 1 and 2) were then weighed, mixed, and placed in the capsules. To allow for liquid expansion and the limitation of powder compaction, only 45 g of salt specimen was placed in each capsule.

The capsules were covered with plastic caps and taken out for transferring into a melting chamber. Three specimens were

handled at a time in this chamber, which was evacuated first before backfilling with argon. The salts were melted and the melting point checked. After solidification, the capsules were removed from the melting chamber, and the cap area was cleaned before final welding. Finally, the special vented end caps were electron-beam welded to the canisters with the frozen salt sample to form the thermal energy storage capsules for the life test.

2.2 *Thermal Cycle Life Test*

Thermal cycle testing was performed to simulate the charge/discharge cycle of any thermal energy storage application by alternately melting and freezing the capsules. This was done in vacuum to reduce the external corrosion of the capsule and to eliminate the possibility of exposure to personnel in the event of a leak. The capsules were stacked inside of a long stainless steel chamber, which in turn was placed horizontally in an electric furnace, as shown in Fig. 1. The temperature gradient (about 50 K from center to ends) of the single-zone-controlled furnace was effectively used to position the high-melting-point samples at the center and the relatively low-melting samples at the ends. A chromel-alumel thermocouple of the sheathed and seated end, attached to each capsule, monitored capsule temperature. A mechanical vacuum pump

Table 1 Purity of Fluoride Salts

Alloy	Grade	Remarks
LiF	Ultrapure(a)	White powder
MgF	Optical grade (99.9%)	Translucent crystals
KF	Ultrapure(a)	White powder
NaF	Ultrapure(a)	White powder

(a) Exceptionally low levels of metallic impurities.

Table 2 Thermal Energy Storage Salt Composition and Melting Points

Eutectic		Weight fraction	Melting point, °C
A	LiF	0.4227	
	MgF_2	0.4876	686 ± 5
	KF	0.0895	
B	LiF	0.3983	
	MgF_2	0.4705	686 ± 5
	NaF	0.1312	
C	LiF	0.4694	
	MgF_2	0.5306	724 ± 5

Source: Ref 3.

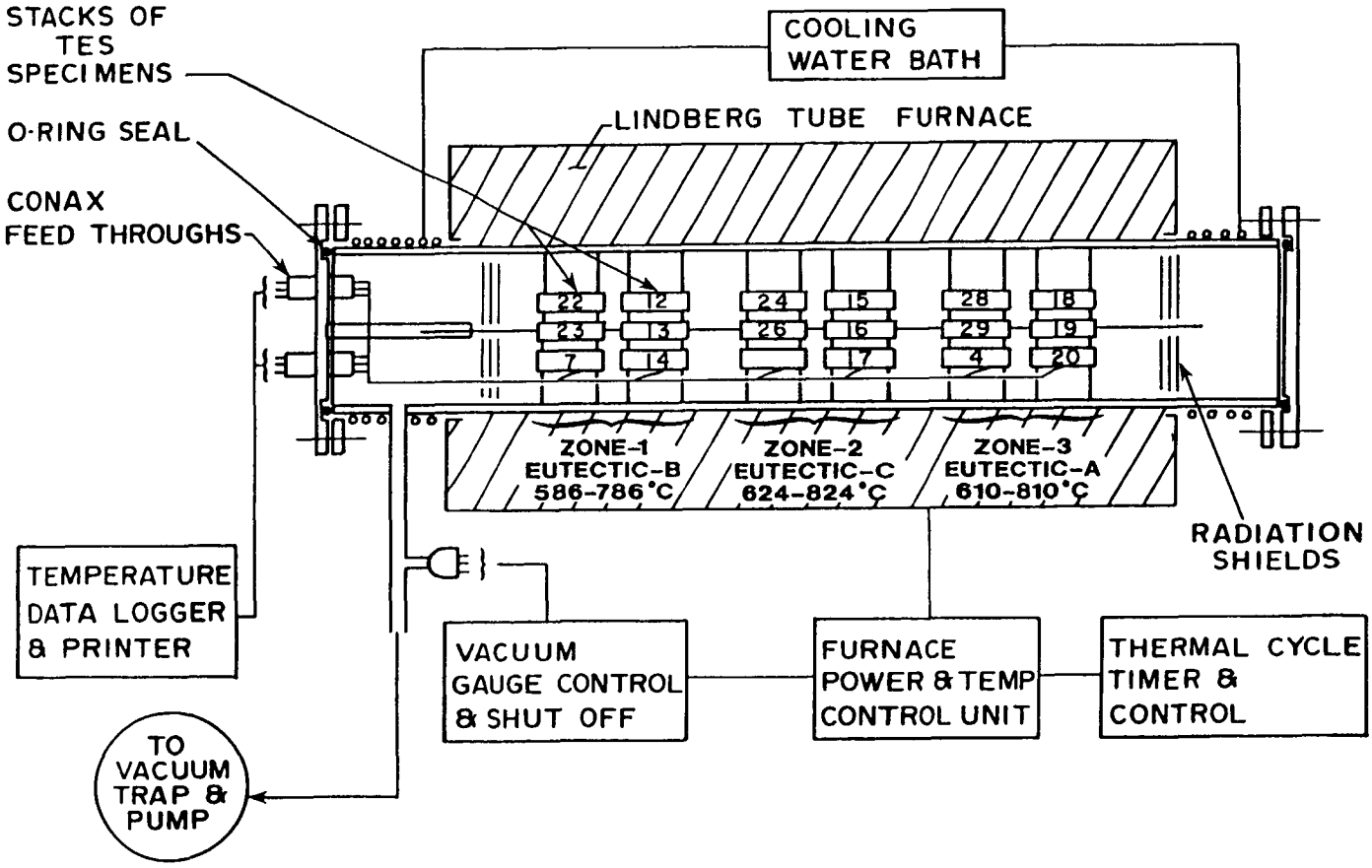

Fig. 1 Schematic setup of thermal energy storage thermal cycle test.

maintained a vacuum of 2.67 N/m^2 (20 mtorr) in the chamber at all times. The electric input of the furnace was controlled by a programmed set point timer, and the cumulative hours and cycles were monitored by counters installed in the circuit.

2.3 *Post-Test Analysis*

Radiography was performed to reveal possible internal flaws and weld defects in the container capsules. Figure 2 shows radiographs taken from samples 13, 16, and 19. The region of higher material density is brighter than the region of lower material density. The solidification profile of the salts is evident in the radiograph. No flaws or defects were observed.

For metallographic examinations, capsules were first sectioned through regions of primary interest. All capsules were initially opened with a hacksaw without the use of cutting fluids. Solidified salt slugs were removed from the containers for chemical analysis, and further container sectioning was done using a water-cooled diamond wafer. End caps were cut off from the capsules, and some were cross-sectioned to evaluate weld integrity.

No general discoloration was found in the salts, but some of the salts had small amounts of dark-colored precipitates. Metallographic specimens of the above capsule sections were prepared by additional fine sectioning and polishing. Scratch-free surfaces were difficult to obtain due to removal of hard inclusions during polishing. After each polishing, the samples were thoroughly washed with distilled water and ethanol and etched by submerging the surfaces in aqua regia for 10 sec.

Metallography of the specimens revealed fairly uniform, fine-grained precipitates in a solid solution matrix. Three types of precipitates were observed—precipitates elongated along the boundaries of grains, small irregularly shaped precipitates distributed within the grains, and large rectangular-shaped orange-colored inclusions. Figure 3 shows the general features of the surfaces. Comparisons between tested and untested samples revealed significant differences in the grain boundary precipitates and the distribution of the grains. Twins were

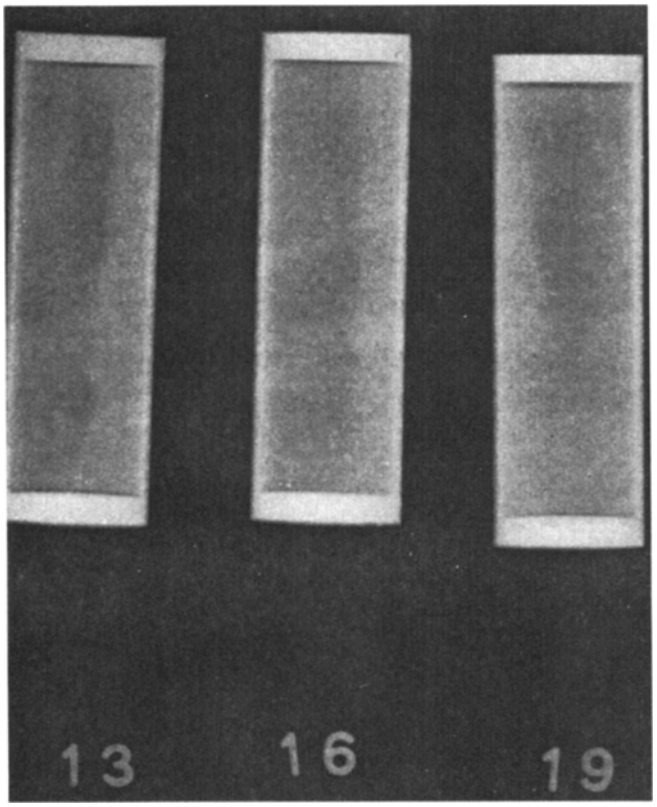

Fig. 2 Radiographs taken from samples 13, 16, and 19 using 350-kV X-ray.

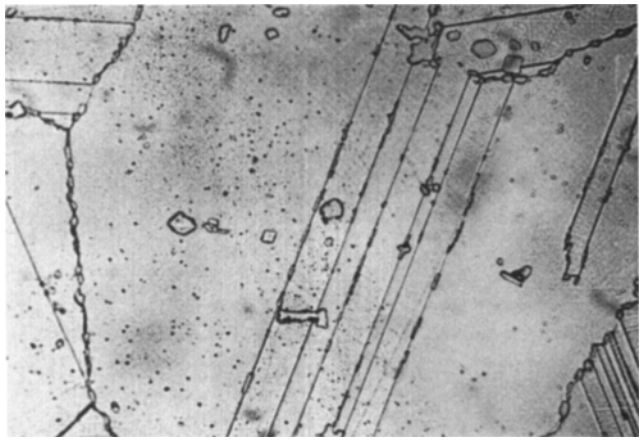

Fig. 3 Optical micrograph showing general features of polished and etched surface (500×).

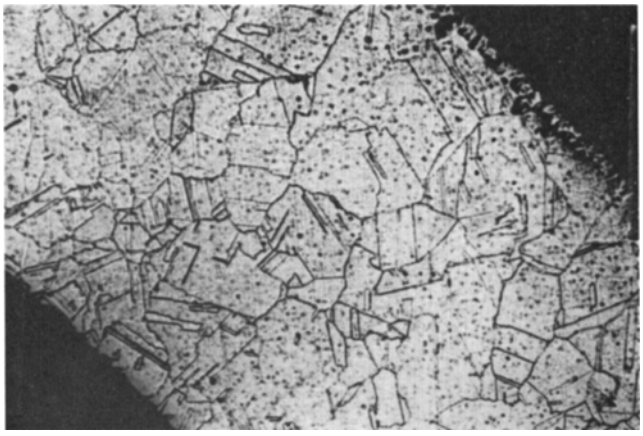

Fig. 4 Optical micrograph showing the tube wall (sample 16 tested for 20,000 hr, 50×).

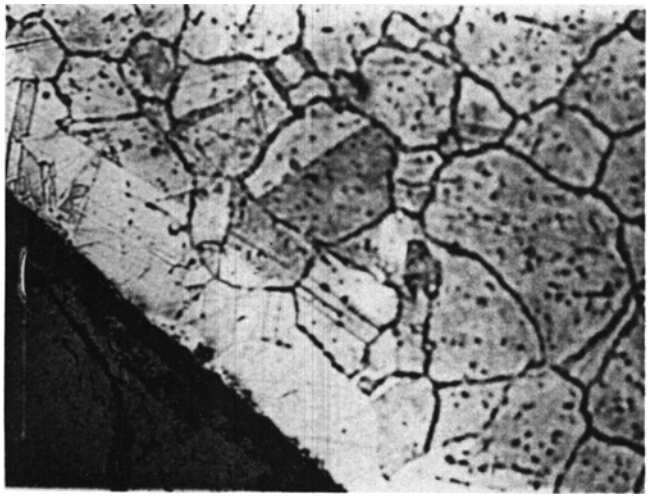

Fig. 5 Optical micrograph showing the outside edge of sample 15 tested for 30,000 hr (200×).

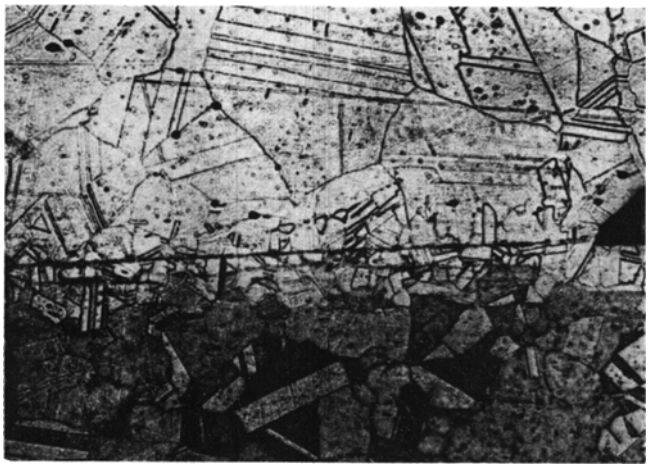

Fig. 6 Optical micrograph showing the gap between the cap and the tube. Note that the gap is perpendicular to the wall.

observed in the grains in multiple numbers. Some of these twins probably were created during heat treatment.

The inner edge exhibited minimal visual damage, as shown in Fig. 4 for samples tested after 20,000 hr. At higher magnifications, small voids were observed near the inner edge. These voids are probably due to salt reactions.

Micrographs of the outer edge reveal more microstructural effects than on the inner edge. Figure 5 shows the outside edge of samples tested under vacuum of 0.06 torr.

Figure 6 illustrates a gap between the cap and the body of the capsule in the welded region. The salts penetrated the unclosed welded areas, but produced only negligible damage to the surface. The microstructure of the cross section near the gap was similar to the other regions, but the grains were slightly smaller than the wall region, as shown in Fig. 7. Some of the gaps in welded areas were perpendicular to the tube wall, which indicates that the cap was not welded properly to the body of the capsule. This weld defect might be the weakest point relative to a pressure buildup inside the capsule.

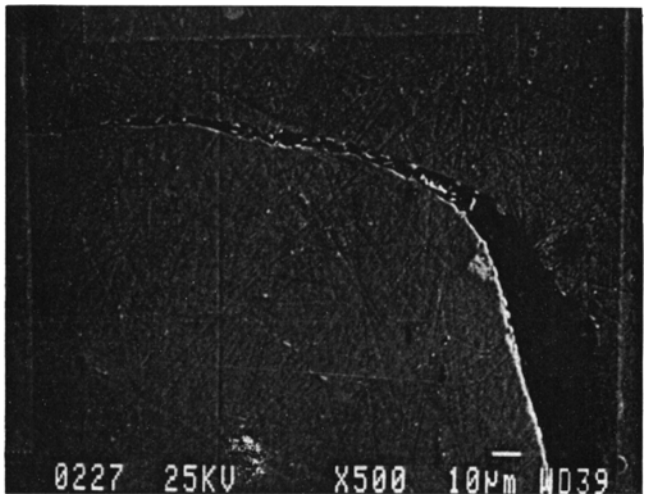

Fig. 7 Optical micrograph showing the microstructure of the alloy near the welded area.

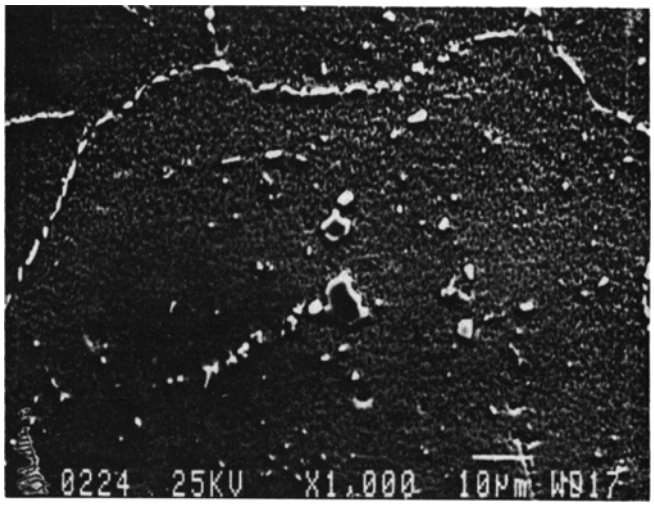

Fig. 8 SEM micrograph taken in the SEI mode showing the precipitate.

Precipitates and inclusions were qualitatively identified by energy dispersive X-ray spectroscopy (EDS). The precipitates along the grain boundaries were either chromium- or molybdenum-rich, and cuboidal precipitates were titanium-rich compounds. Secondary electron images (SEI) of these precipitates are shown in Fig. 8 to 10. It was known that the untested Inconel 617 samples did not have grain-boundary precipitates, and the distribution of these precipitates was more random than the precipitates in tested samples. Therefore, the grain-boundary precipitates were formed during thermal cycle testing and were most probably carbide compounds of chromium and molybdenum based on EDS analysis.

The inner edges of the cut specimens were examined by scanning electron microscopy (SEM). Figures 11 to 13 show the extent of the damage done to the inner edge by eutectic salts at high temperature. The images show that there are no precipitates at grain boundaries within 50 and 70 μm of the edge for

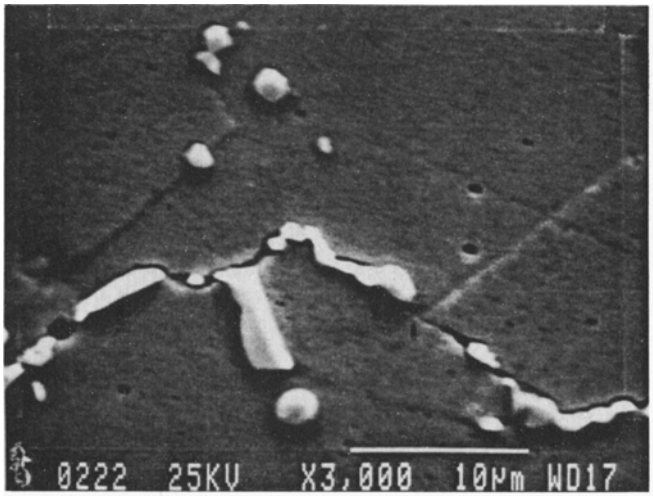

Fig. 9 SEM micrograph taken in the SEI mode showing the elongated precipitates at the grain boundary.

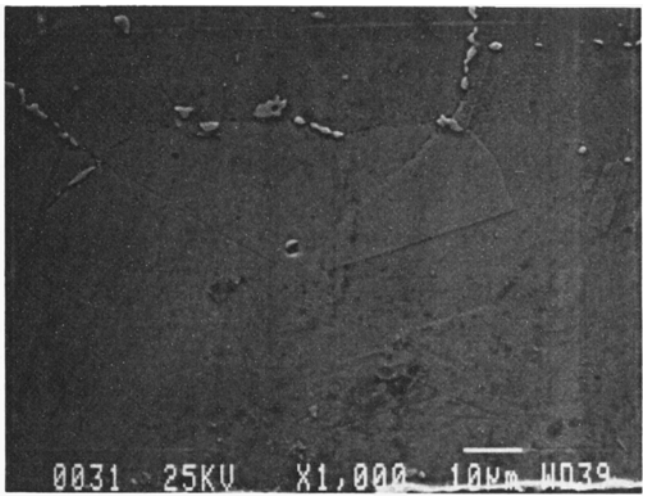

Fig. 11 SEM micrograph showing the inside edge (sample 12 tested for 30,000 hr).

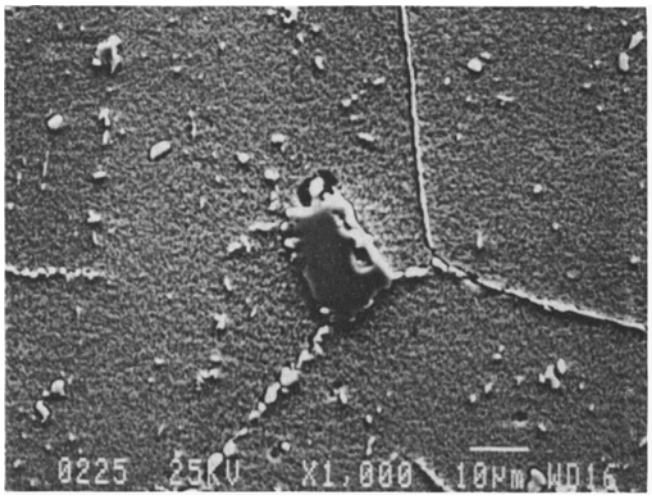

Fig. 10 SEM micrograph of titanium-rich precipitate attached to grain boundary.

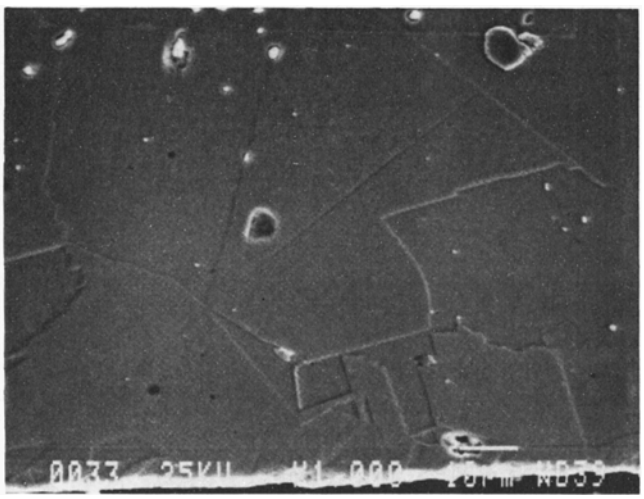

Fig. 12 SEM image of inside edge (sample 16 tested for 20,000 hr, salt type C).

samples tested 20,000 and 30,000 hr, respectively. There were some voids in the precipitate-depleted region, which may be due to the polishing process or diffusion of alloying elements from the surfaces. These voids may have resulted from vacancies created by preferential diffusion of chromium and aluminum into the salts.

Figures 14 to 16 show the near-surface region at the outer edge (exposed to 0.06 torr vacuum). Microstructural changes are apparent to a depth of 70 to 120 µm after 20,000 and 30,000 hr, respectively.

The variation in concentration of each alloying element was measured by electron probe microanalysis (EPMA) across the wall thickness at 10- and 20-µm intervals from the inside and outside edges. This was done to assess the depletion of alloying elements. The probe beam must impinge on a flat surface for accurate results. Therefore, areas close to rounded edges could produce erroneous values from a loss of signal. Spots near the precipitates and voids were not measured to prevent signal interference from the bulk analysis.

Concentrations of aluminum, chromium, and molybdenum were plotted as a function of position. The results are shown in Fig. 17 to 20. A decrease from the nominal composition is observed for aluminum and chromium near the edges. The composition then matches the nominal composition deeper into the wall. The molybdenum composition varies in a manner opposite to aluminum and chromium. The molybdenum composition is above the nominal value near the outside edge, drops below nominal, and then increases back to the nominal composition again. This behavior suggests that molybdenum diffuses from the matrix to the surface, but does not evaporate. The graphs for aluminum and chromium suggest that they both diffuse to the surface and then react with the salt on the interface. To verify this reaction, chemical analyses were performed for traces of aluminum and chromium in the salt. The quantitative

analysis of the salts for aluminum and chromium was performed using atomic absorption spectroscopy (AAS) with standards. The salt samples were dissolved in nitric acid. The results are presented in Table 3.

Detection of surface reaction products was performed with X-ray diffraction on the inside surface of the tube. X-ray diffraction analysis was conducted on the flat inside surface of the end cap. After subtracting the background Inconel 617, some small peaks were left to be analyzed. The *d*-spacings and the relative intensities of the peaks were compared with standards from the chemical compound files that matched the compounds $NaMgF_3$ and MgF_2, with an accuracy of 0.1 for the *d*-spacing. Aluminum compounds could not be detected, although their presence is likely because the complex compounds of $MAlF_6$ (where *M* is lithium, potassium, or sodium) were not listed in the compound files. If an aluminum compound film is formed on the inside surface, the reduction of the aluminum in the salt (Table 3) is then explained.

3. Discussion

Metallographic examination of specimen cross sections did not reveal any significant change in the microstructure of the Inconel 617. The most important difference in tested and untested Inconel 617 was the presence of molybdenum-rich precipitates in the tested samples. This suggests that carbides were probably formed during long exposure to high temperatures, especially near the sensitization range. Comparison of micrographs taken from the 20,000- and 30,000-hr tested samples revealed the following differences. The depth from the inside edge, which was free of precipitates, was 80 to 90 μm for

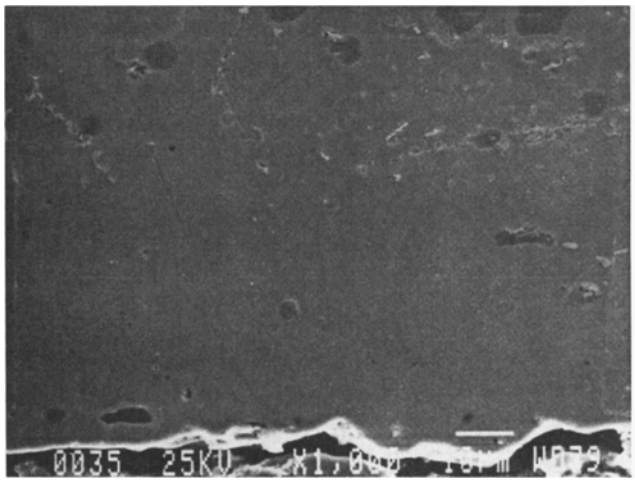

Fig. 13 SEM image of inside edge (sample 19 tested for 20,000 hr, salt type A).

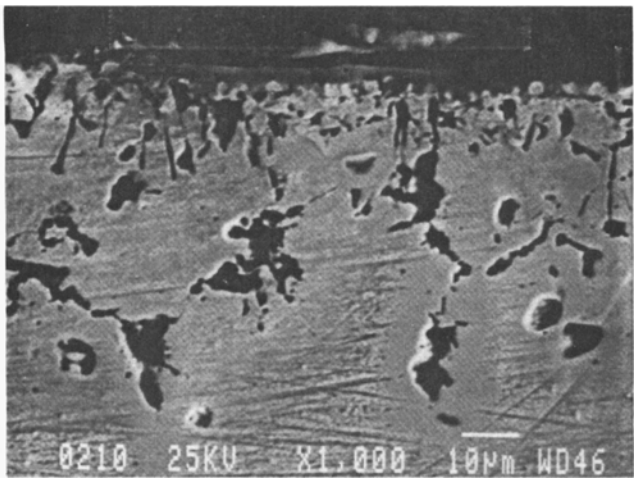

Fig. 14 SEM micrograph showing the outside edge of sample 13 tested for 20,000 hr.

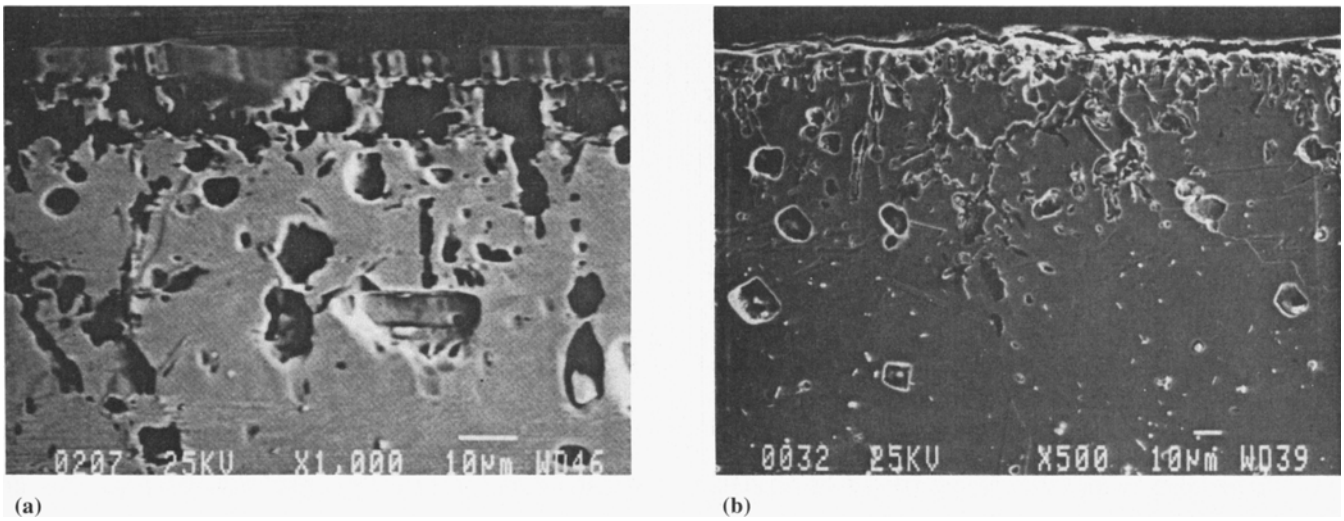

Fig. 15 SEM micrograph showing the outside edge. **(a)** Sample 16 tested for 20,000 hr. **(b)** Sample 15 tested for 30,000 hr.

20,000-hr samples and 130 to 150 μm for 30,000-hr samples. The depth of microstructural changes from the outside edge (vacuum 0.06 torr) was 60 to 70 μm for 20,000-hr sample and 110 to 120 μm for 30,000-hr samples.

Some samples showed more surface effects than others; for example, micrographs of sample 12 (30,000 hr, eutectic B) showed no visible demarkation along grain boundaries over a depth of 600 μm from the outside edge. These observations suggest that precipitates of molybdenum and chromium were dissolved by the matrix as the respective elements were evaporated at the outside edge. Also, at the inside edge, precipitates of aluminum and chromium were depleted because of reactions with salt. These observations did not give much insight into the mechanisms of corrosion. Further analyses were performed to evaluate the true nature of the corrosion mechanism.

Quantitative analysis was needed to more accurately describe the compositional changes along the tube wall, especially in regions close to the inside and outside edges. EPMA measurements were therefore made across the wall of the container starting from the inside and outside edges and moving inward in 10- and 20-μm increments. The microprobe measurements revealed a decrease in the percentage of aluminum and chromium relative to their nominal value near the inner edge in contact with the salt. The data obtained by the probe may reflect measurement errors due to probe size and pits at the points of observation. Also, data points near the edge (0 to 10 μm from the edge) were not accurate due to loss of signals. Semiquantitative analysis is still possible using these measurements. Furthermore, chemical analysis of the salts by atomic absorption spectroscopy, which showed small amounts of aluminum and traces of chromium, supports the conclusions from the microprobe measurements.

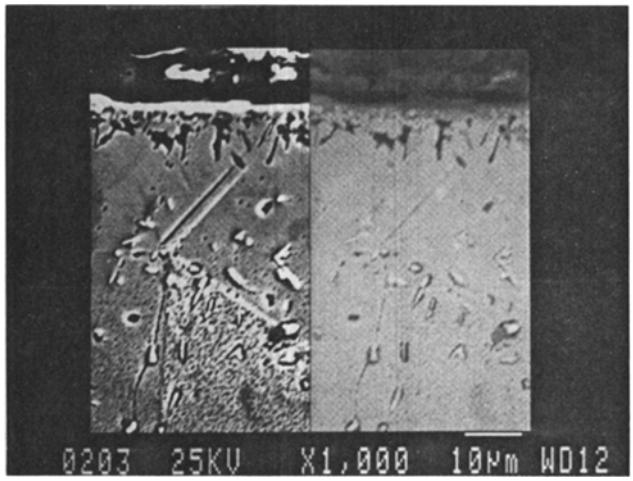

Fig. 16 SEM micrographs (SEI, left; BSE, right) taken from the outside edge (sample 19 tested for 20,000 hr).

Thermodynamic calculations by Misra and Whittenberger[6] predict this behavior of aluminum and chromium. In their calculations, the reaction of one mole of LiF, KF, NaF, or MgF_2 with pure metals, assuming ideal and nonideal conditions, were needed. The equilibrium amount of aluminum salts is the highest, followed by that of chromium salts. The assumed reactions are:

$$6MF_{(l)} + Al \rightarrow M_3AlF_{6(l)}$$

$$2MF_{(l)} + Al \rightarrow CrF_2 + 2M_{(l)}$$

where M is lithium, potassium, or sodium, and

$$3MgF_{2(l)} + 2Al \rightarrow 2AlF_{3(l)} + 3Mg_{(s)}$$

$$MgF_2(l) + Cr \rightarrow CrF_2(l) + Mg_{(s)}$$

Calculations for the equilibrium amounts were made by Misra and Whittenberger,[6] who have reported the following values; 0.1 mole of M_3AlF_6 forms with every mole of NaF or KF, whereas 0.001 mole of the salt forms with one mole of LiF. The amounts of aluminum determined by these calculations for the present work are 0.4 wt.% in A, 0.89 wt.% in B, and 0.05 wt.% in C. These values are approximate based on the assump-

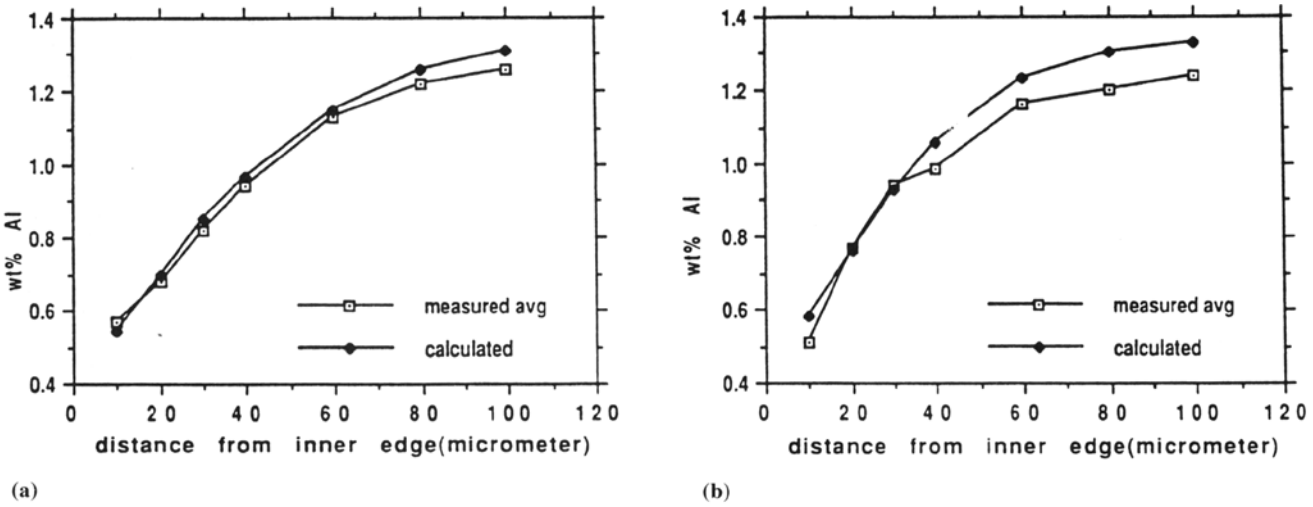

Fig. 17 Concentration profile of aluminum vs the distance from inside edge (salt type A). **(a)** Samples tested after 20,000 hr of cycling. **(b)** Samples tested after 30,000 hr.

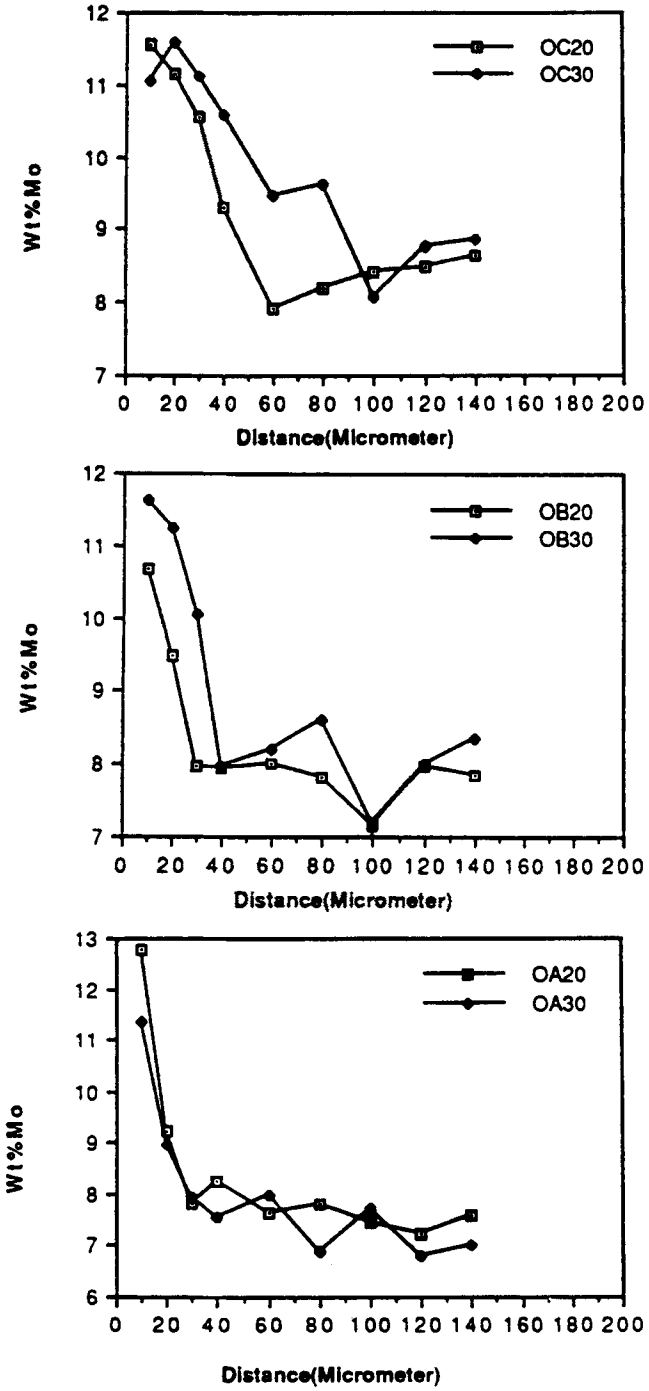

Fig. 18 Concentration profile of aluminum vs the distance from outside edge. O ≡ outside; A ≡ type A; B ≡ type B; C ≡ type C; 20 ≡ 20,000 hr; 30 ≡ 30,000 hr.

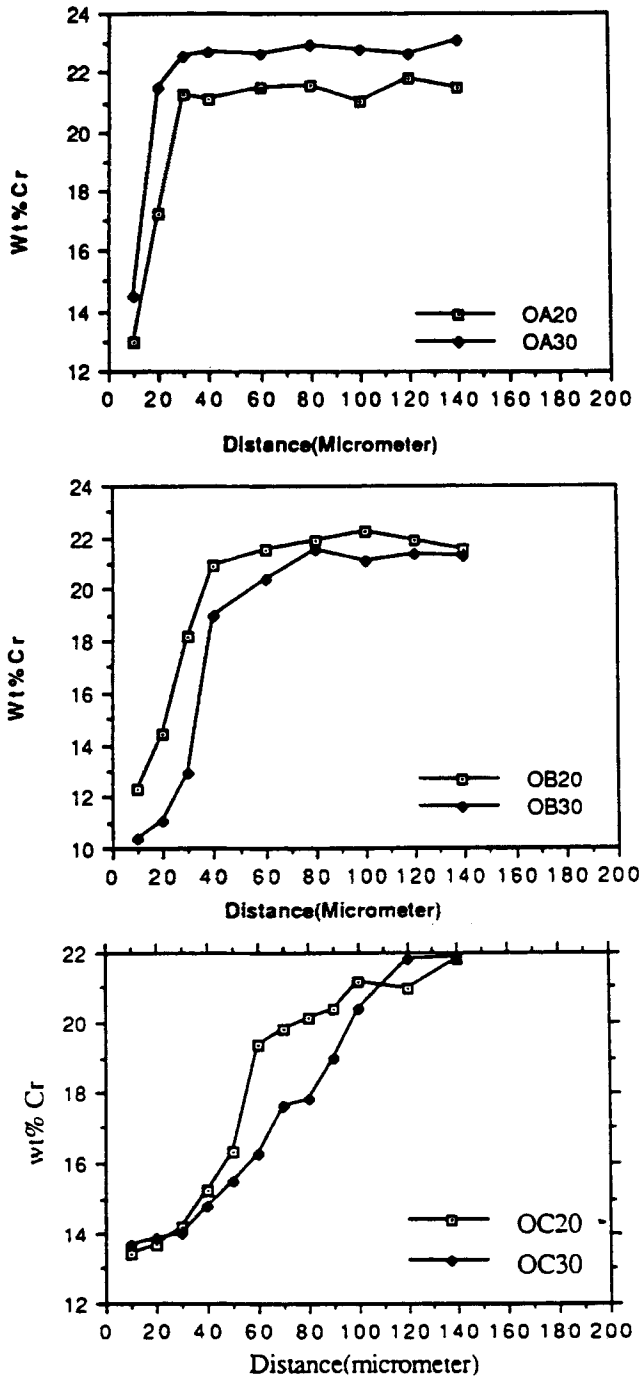

Fig. 19 Concentration profile of chromium vs the distance from outside edge. O ≡ outside; A ≡ type A; B ≡ type B; C ≡ type C; 20 ≡ 20,000 hr; 30 ≡ 30,000 hr.

tion of ideal conditions. The amounts of aluminum determined from AAS measurements for samples tested after 30,000 hr of cycling were 0.28 wt.% in A, 0.17 wt.% in B, and 0.13 wt.% in C, as shown in Table 3.

In other calculations by Misra and Whittenberger[6] for nonideal conditions, calculated molar quantities of the metallic salt increase by an order of magnitude. An activity coefficient of 0.001 for AlF_3 and 0.1 for Mg would yield equilibrium values for aluminum salt of 0.93 wt.% for A, 1.3 wt.% for B, and 0.55 wt.% for C.

The weight percentage of aluminum determined from AAS measurements decreased as the testing time increased. This decrease may be explained by the formation of the corrosion product layer on the inside surface of the tube.

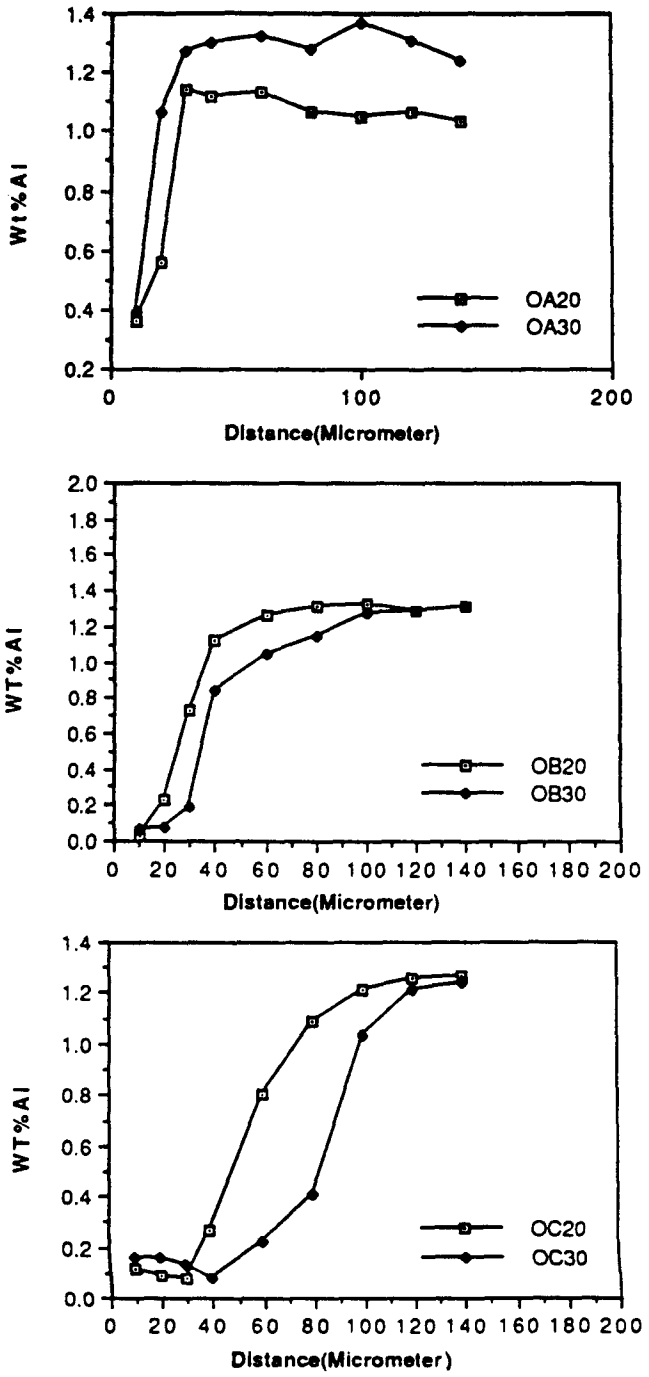

Fig. 20 Concentration profile of molybdenum vs the distance from outside edge. O = outside; A = type A; B = type B; C = type C; 20 = 20,000 hr; 30 = 30,000 hr.

A concentration profile of aluminum across the tube wall near the inner edge is shown in Fig. 18. Krishnamurthy *et al.*[4] modeled the data for 10,000-hr tested samples as a diffusion curve of a binary system in a one-dimensional semi-infinite bar. Their model results in a $D = 1.0 \times 10^{-13}$ cm^2/sec and C_s = 0.38 wt.% aluminum, where D is the diffusion coefficient of aluminum in the alloy and C_s is the aluminum concentration at the salt-clad interface.

Using these values of C_s and D in the diffusion equation for test times of 20,000 and 30,000 hr, the following were obtained:

$$C_x = C_s + (C_o - C_s) \text{ erf } (0.5\ (D_t)^{-1/2})$$

where C_x is the concentration (wt.%) of aluminum at a distance x from the inner edge; C_s is the concentration at the surface (x = 0, 0.38); C_o is the concentration in the bulk alloy; D is the diffusion coefficient of aluminum in the alloy (1.0×10^{-13} cm^2/sec); x is the distance measured from the inner edge of the capsule wall; and t is the testing time.

Substituting D and C_s values in the equation yields:

$$C_x = 0.38 + 0.96 \text{ erf } [1.58 \cdot 10^6(t)^{-1/2}x]$$

Table 4 lists the measured averages from microprobe analysis and calculated values of C_x at various positions from the inner edge. Comparison of these values is shown in Fig. 17. Considering the possible errors in measurements, the measured values are in good agreement with the calculated values. Therefore, it might be concluded that corrosion of this form is a solid-state diffusion-dominated process.

As shown in Fig. 17 and 18, the corrosion process is not controlled by thermodynamic reactions on the salt-clad interface. Diffusion plays an important role in the development of the corrosion process.

Depletion of chromium from the alloy is also observed from the data obtained by EPMA analysis across the wall. However, it is almost negligible compared to the amount of chromium in the alloy. This is also evident from the chemical analysis of the salts. The amount of chromium in the salt was on the order of 10^{-4} wt.% of the salt. Because the chromium diffusion and reaction with the salt is very small, depletion of chromium is negligible compared to aluminum. Consequently, it can be concluded that chromium depletion is not expected to cause severe degradation in alloy properties.

The outer edge of the specimen exhibits more damage than the inner edge. Because the capsules were exposed to 0.06 torr vacuum at high temperature, diffusion and evaporation of some elements in the alloy were expected. The micrographs show subsurface spherical voids and some crack shape damage on the surface. The concentrations obtained along the wall thickness show a strong depletion of aluminum and chromium.

Figures 19 and 20 illustrate the relationship between alloy content (aluminum and chromium) versus the distance from the outer edge. The best explanation for outside damage would be the diffusion and vaporization of the elements into the vacuum. Vapor pressures of the gaseous elements at 1100 K increase on the order of molybdenum, cobalt, nickel, chromium, and aluminum. The high vapor pressures of aluminum and chromium relative to that of nickel, cobalt, and molybdenum suggest that the high-temperature vacuum would produce a sizeable aluminum and chromium gradient. The appreciable decrease in aluminum content from 1.35% to 0.1% and in chromium content from 21.8% to as low as 10% was an indication that the theoretical predictions were accurate.

The formation of voids could be explained principally by the movement of vacancies, that is, neighboring atoms move to occupy vacant sites. This gives the illusion that the vacancy it-

Table 3 Composition of Aluminum and Chromium in Tested Salts

	Chromium			Aluminum		
	Composition, wt.%, of eutectic salt type:					
Cycling time, hr	A	B	C	A	B	C
10,000	0.00034	0.00043	0.00043	0.31	0.25	0.29
20,000	0.00113	0.00077	0.00056	0.24	0.17	0.16
30,000	0.00046	0.00129	0.00019	0.28	0.17	0.13

Table 4 Calculated and Measured Averages of Aluminum Content Across the Wall from the Inside Edge

	Measured average, wt.%		Calculated, wt.%	
Distance,	Hours tested:			
μm	20,000	30,000	20,000	30,000
10	0.51	0.57	0.58	0.54
20	0.77	0.68	0.76	0.70
30	0.94	0.82	0.93	0.85
40	0.99	0.94	1.06	0.97
60	1.16	1.13	1.23	1.15
80	1.20	1.22	1.30	1.26
100	1.24	1.26	1.33	1.31

self is moving in the opposite direction. When the atoms on the surface are vaporized, the atoms below the surface move to occupy the vacancy, which in turn creates a vacancy under the surface. This process moves the vacancies to the subsurface, and by the clustering of vacancies, subsurface voids are formed. Cracks on the surface could be due to polishing, and the weakened surface could have been removed by polishing particles.

Some of the capsules exhibited a gap between the tube and the end cap perpendicular to the wall. This indicates a lack of penetration of the weld. These gaps might become the weakest points of the capsule, leading to a failure if the thermal cycle test continued. Increasing welding penetration, or changing cap design, is suggested.

4. Conclusions

The thermal energy storage capsules removed after 20,000 and 30,000 hr of freeze/thaw cycle testing showed no significant degradation, and their microstructure was still stable, except for the effects of aging. The salt-clad interfaces exposed for 30,000 hr showed a small increase in damage compared to those tested for 20,000 hr (30 to 40 μm more). The amount of aluminum in the salt actually decreased as the testing time increased, or stayed almost constant. This suggests that a film of fluoride compounds of aluminum, chromium, or some other alloying elements may have formed on the surface. The concentration profile of aluminum across the tube wall from the inside edge closely followed the diffusion equation derived for the current problem based on the assumption of constant surface concentration and a one-dimensional semi-infinite bar. The diffusion coefficient of 10^{-13} cm^2/sec and surface concentration of 0.38 was based on the diffusion model obtained for samples tested 10,000 hr. Average measured values from microprobe analysis for 20,000- and 30,000-hr tested samples closely fit the model, with an error bar of 5 to 7%. These results suggest that the corrosion process was controlled by solid-state diffusion in the alloy.

The container material chosen for this particular purpose was found to be adequate. Reduction of aluminum in the alloy, without affecting the mechanical properties of the container, would yield a less corrosive candidate for thermal energy storage capsules. This reduction in percentage of aluminum is also beneficial in reducing the damage to the outside (exposed to vacuum), because aluminum has highest rate of vaporization among the alloying elements. The effect of oxidation was ignored, because these capsules will be operating in space.

Overall performance of the capsules resisting the corrosive environment was very good for the cumulative time duration they had been tested (30,000 hr). The projected lifetime of 5 to 7 years is thus reasonable.

Acknowledgments

This research was supported by the Aero Propulsion and Power Directorate, Wright Laboratory, Wright-Patterson Air Force Base, Ohio. The authors would like to thank Dr. E.T. Mahefkey for his advice at various stages of this study.

References

1. W.E. Simon, *Proceedings of 19th Intersociety Energy Conversion Engineering Conference (IECEC)*, Aug 1984, p 324.
2. A.K. Misra, *J. Electrochem. Soc.*, Apr 1988, p 850.
3. R. Ponnappan, J.E. Beam, V.J. Van Griethuysen, and E.T. Mahefkey, *Proceedings of 20th Intersociety Energy Conversion Engineering Conference (IECEC)*, Aug 1985, Vol 2, p 416-423.
4. M. Krishnamurthy, D.L. Jacobson, R. Ponnappan, and J. Johnson, *J. Mater. Eng.*, Vol 11 (No. 4), 1989, p 283.
5. J.W. Koger, *Adv. Corrosion Sci. Technol.*, Vol 5, 1975, p 245.
6. A.K. Misra and J.D. Whittenberger, *Proceedings of 22nd Intersociety Energy Conversion Engineering Conference (IECEC)*, Aug 1987, p 188.
7. D.L. Jacobson, Technical Report No. AFAPL-TR 77-9, 1976.